J. Fluid Mech. (1992), *vol.* 241, *pp.* 291–309
Printed in Great Britain

Multiple equilibria in two-dimensional thermohaline circulation

By PAOLA CESSI[1,2] AND W. R. YOUNG[2]

[1] Istituto FISBAT-CNR, I-40126 Bologna, Italy

[2] Scripps Institution of Oceanography, La Jolla, CA 92093, USA

(Received 22 November 1991 and in revised form 17 January 1992)

As a model of the thermohaline circulation of the ocean we study the two-dimensional Boussinesq equations forced by prescribing the surface temperature and the surface salinity flux. We simplify the equations of motion using an expansion based on the small aspect ratio of the domain. The result is an amplitude equation governing the evolution of the depth averaged salinity field. This amplitude equation has multiple, linearly stable equilibria. The simplified dynamics has a Lyapunov functional and this variational structure permits a simple characterization of the relative stability of the alternative steady solutions.

Even when the thermal and salinity surface forcing functions are symmetric about the equator there are asymmetric solutions, representing pole to pole circulations. These asymmetric solutions are stable to small perturbations and are always found in conjunction with symmetric solutions, also stable to small perturbations. Recent numerical solutions of the full two-dimensional equations have shown very similar flow patterns.

1. Introduction

At present the ocean circulation is thermally direct: cold water sinks at the poles and rises at the equator. The bottom water is cold and fresh. But palaeoceanographic datasets have suggested that in the past the sense of the circulation has been reversed, so that warm salty water sank near the equator and cold fresh water upwelled at the poles. The bottom water was warm and salty. Kennett & Stott (1991) report evidence from sediment records of an abrupt reversal in the oceanic sub-thermocline meridional cell. In their interpretation of the data, saline warm water from the midlatitudes and tropics sank to the deep ocean and spread to Antarctica where bottom water formation was suppressed. Broecker, Peteet & Rind (1985) have proposed a similar circulation reversal during glacial times in the North Atlantic, leading to a suppression of polar deep-water formation.

The existence of more than one equilibrium circulation is understandable if one considers that the latitudinal distributions of thermal and saline forcing at the ocean surface are antagonistic in their effects on the density field. Colder temperatures in high latitudes favour sinking near the poles, while fresh water fluxes there tend to prevent it.

The analysis of simple box models, such as those proposed by Stommel in 1961, has shown that the existence of multiple equilibria requires 'mixed boundary conditions' for the temperature and salinity. This means that the boundary conditions cannot be translated into a prescription for density alone (Welander 1986). This difference

arises at the air–sea interface because the thermal flux depends strongly on the ocean temperature, while the saline flux is essentially independent of the salt concentration.

The meridional thermohaline circulation of a single ocean has several different stable states:

(i) The circulation is dominated by the thermal surface forcing and has a cell in each hemisphere with water sinking at the poles and rising at the equator.

(ii) The circulation is predominantly driven by surface salinity flux and has a cell in each hemisphere with water sinking at the equator.

(iii) The flow is driven by a combination of thermal and saline forcing and a single pole-to-pole cell results. In this case two states are possible: one with sinking at the north pole and the other with sinking at the south pole.

In his review Welander (1986) illustrates these four equilibria using a three-box model in which the connection between the reservoirs is by hydraulic pipes. Two boxes represent the polar and subtropical section of each hemisphere and the third box is a proxy for the equatorial and subtropical region. In the effort to increase both the vertical and horizontal resolution, many variations and elaborations of box models can now be found in the literature. Unfortunately the twin advantages of conceptual simplicity and analytic tractability are lost as the plumbing becomes more intricate. And it is not clear that multiple box models are 'closer' to the true dynamics than the two-box model originally proposed by Stommel (1961).

As an alternative to box models, multiple equilibria are also found in complex general circulation models (GCMs) of the ocean (Bryan 1986) and of the coupled ocean–atmosphere system (Manabe & Stouffer 1988). In Bryan (1986) the surface flux conditions for salt and temperature are specified. On the timescales relevant to climate change the Rayleigh-type boundary condition for temperature is equivalent to a fixed-temperature prescription and Bryan demonstrates that the model has multiple stable equilibria.

A model of intermediate complexity between box-models and GCMs has been analysed by Thual & McWilliams (1991). They consider the two-dimensional non-rotating Navier–Stokes equations forced by prescribed surface temperature and salinity flux. Numerical solutions of the equations exhibit the equilibria listed above and Thual & McWilliams (1991) determine the range of forcing parameters for which these multiple equilibria are obtained.

In this article we use the same intermediate model employed by Thual & McWilliams, but we analyse it in a particularly tractable limit in which it is possible to take advantage of the extremely small aspect ratio of the domain. We expand in a small parameter which is the ratio of the vertical to horizontal lengthscales. This approach to convection with flux boundary conditions has previously been employed by Chapman & Proctor 1980, Depassier & Spiegel 1982 and Roberts 1985. The asymptotic development used here is similar in spirit, but the details of the scaling are different.

Specifically we assume that the surface forcing is of small enough amplitude that diffusion dominates the lowest-order balance. This restriction permits analytical progress, but constrains the temperature and salinity fields to be vertically homogenous to a first approximation. Of course vertical stratification is an essential ingredient both in the ocean and in general circulation models. However, the simple limit analysed here reproduces qualitatively the equilibria listed above and permits an easy characterization of the solutions.

2. Equation of motion and non-dimensionalization

We consider the two-dimensional, Boussinesq equations for a fluid whose motion is driven by temperature and salinity gradients. In standard notation the equations of motion are:

$$\partial_t v + v\,\partial_y v + w\,\partial_z v = -\partial_y p + \nu\nabla^2 v, \tag{2.1a}$$

$$\partial_t w + v\,\partial_y w + w\,\partial_z w = -\partial_z p - g(\alpha_S S - \alpha_T T) + \nu\nabla^2 w, \tag{2.1b}$$

$$\partial_y v + \partial_z w = 0, \tag{2.1c}$$

$$\partial_t T + v\,\partial_y T + w\,\partial_z T = \kappa_T \nabla^2 T, \tag{2.1d}$$

$$\partial_t S + v\,\partial_y S + w\,\partial_z S = \kappa_S \nabla^2 S. \tag{2.1e}$$

The motion is in the (y, z)-plane. This simplified model captures certain features of the zonally averaged meridional circulation driven by thermohaline forcing. It does not, however, include the effects of rotation and vertical vorticity, which are paramount in the wind-driven ocean circulation.

The density ρ is related to the temperature, T, and salinity, S, through the equation of state, which we take to be linear:

$$\rho = \rho_0(1 + \alpha_S S - \alpha_T T). \tag{2.2}$$

Because the motion is two-dimensional, we introduce a stream function, ψ, so that

$$v = -\partial_z \psi, \quad w = \partial_y \psi. \tag{2.3}$$

The pressure field can be eliminated by forming the vorticity equation, and the flow is then governed by:

$$\left.\begin{aligned} \partial_t \nabla^2\psi + J(\psi, \nabla^2\psi) &= g(\alpha_T\,\partial_y T - \alpha_S\,\partial_y S) + \nu\nabla^4\psi, \\ \partial_t T + J(\psi, T) &= \kappa_T \nabla^2 T, \\ \partial_t S + J(\psi, S) &= \kappa_S \nabla^2 S. \end{aligned}\right\} \tag{2.4}$$

We assume that our model ocean is contained in a rectangular box with coordinates $0 \leqslant z \leqslant d$, and $-l \leqslant y \leqslant l$. The forcing is provided by the top boundary conditions on temperature and salinity. As discussed by Bryan (1986) the salinity and temperature fields are forced very differently at the top boundary. Because the heat flux between the atmosphere and the ocean depends strongly on the sea surface temperature, the temperature at the interface tends to adjust to an equilibrium value. In a simple model, such as ours, where the ocean is decoupled from the atmosphere, this amounts to specifying the temperature at the ocean top, $z = d$. On the other hand, the ocean surface salinity has almost no effect on the rate of precipitation and evaporation, and, in a decoupled model, it is appropriate to specify the salinity flux at the ocean surface. We further assume that the solid earth at the bottom and on the sides of the ocean is a poor conductor so both the temperature and salinity fluxes vanish there. In summary we have the following boundary conditions for T and S

$$\left.\begin{aligned} T(y, d) = \Delta T\theta(y), \quad \partial_z S(y, d) &= \Delta S F(y)/d, \\ \partial_z T(y, 0) = 0, \quad \partial_z S(y, 0) &= 0, \\ \partial_y T(\pm l, z) = 0, \quad \partial_y S(\pm l, z) &= 0. \end{aligned}\right\} \tag{2.5}$$

Here ΔT and ΔS are dimensional constants characterizing the magnitude of the forcing. $\theta(y)$ and $F(y)$ are non-dimensional functions whose magnitude is normalized to unity by the choice of ΔT and ΔS. Because we neglect mechanical forcing the

boundary conditions for the streamfunction are homogeneous on all boundaries. Thus ψ is zero on the boundary and it also satisfies either no-slip or no-stress. In the discussion to follow it will become clear that the choice of no-slip versus no-stress makes little difference to the results.

The system (2.4) with boundary conditions (2.5) is best dealt with in non-dimensional variables (denoted for the moment by $'$). We use the definitions

$$(y,z) = d\left(\frac{y'}{\epsilon}, z'\right), \quad t = \frac{d^2}{\kappa_T} t', \quad \psi = \frac{\kappa_T}{\epsilon}\psi', \quad T = T' \frac{\nu\kappa_T}{g\alpha_T d^3\epsilon^2}, \quad S = S' \frac{\nu\kappa_T}{g\alpha_S d^3\epsilon^2}. \tag{2.6}$$

In (2.6) we have introduced the aspect ratio

$$\epsilon \equiv \frac{\pi d}{l}. \tag{2.7}$$

Dropping all the primes, (2.4) becomes in non-dimensional variables:

$$\left.\begin{aligned} P^{-1}[\partial_t \zeta + J(\psi,\zeta)] &= \partial_y T - \partial_y S + (\partial_z^2 + \epsilon^2\partial_y^2)\zeta, \\ \partial_t T + J(\psi, T) &= (\partial_z^2 + \epsilon^2\partial_y^2) T, \\ L^{-1}[\partial_t S + J(\psi, S)] &= (\partial_z^2 + \epsilon^2\partial_y^2) S, \end{aligned}\right\} \tag{2.8}$$

where $\zeta \equiv (\partial_z^2 + \epsilon^2\partial_y^2)\psi$. We have denoted with $P \equiv \nu/\kappa_T$ the Prandtl number and with $L \equiv \kappa_S/\kappa_T$ the Lewis number. The motion is now contained in the domain $0 \leqslant z \leqslant 1$ and $-\pi \leqslant y \leqslant \pi$. The inhomogeneous boundary conditions for the temperature and salinity fields are

$$T(y,1) = a\theta(y), \quad \partial_z S(y,1) = bF(y). \tag{2.9}$$

Here a and b are the non-dimensional numbers introduced by Thual & McWilliams

$$a \equiv \frac{g\alpha_T \Delta T d^3\epsilon^2}{\nu\kappa_T}, \quad b \equiv \frac{g\alpha_S \Delta S d^3\epsilon^2}{\nu\kappa_T}. \tag{2.10}$$

These parameters are essentially the thermal and saline Rayleigh numbers.

In summary, there are five dimensionless parameters: a, b, P, L and ϵ. There are also two externally prescribed functions which enter through the boundary conditions at $z = 1$ namely $T(y,1) = a\theta(y)$ and $\partial_z S(y,1) = bF(y)$.

3. The expansion

For oceanic applications, the aspect ratio, ϵ, is very small and we seek an expansion in this parameter so that analytic progress can be made. Because no mechanical forcing is imposed, motion occurs in response to the density gradient prescribed at the surface. The analysis of the linear problem in Thual & McWilliams suggests that if the amplitude of the surface salinity flux is related to the surface temperature by the relation

$$b \sim \epsilon^2 a, \tag{3.1}$$

then the temperature and salinity contribution to the density field are of the same order. We further assume that a is of the order of ϵ and we consider a distinguished limit in which $\epsilon \to 0$ and

$$a = \epsilon a_1, \quad b = \epsilon^3 b_3, \tag{3.2}$$

where a_1 and b_3 are held fixed. All the fields are expanded in powers of ϵ:

$$(\psi, T, S) = \epsilon(\psi_1, T_1, S_1) + \epsilon^2(\psi_2, T_2, S_2) + \ldots, \tag{3.3}$$

and the time is rescaled by $t_2 = \epsilon^2 t$ so that

$$\partial_t = \epsilon^2 \partial_{t_2}. \tag{3.4}$$

The scalings for a and b in (3.2) require that T_1 must be equal $a_1\theta(y)$ at $z = 1$, and all of the other terms in the expansion of T vanish at this upper boundary. However, for the salinity it is $\partial_z S_3$ which satisfies the flux condition at $z = 1$. The earlier terms in the expansion, $\partial_z S_1$ and $\partial_z S_2$, are both zero at the upper boundary.

3.1. *The first-order solution*

Collecting the terms of order ϵ we have the system

$$\left.\begin{aligned} 0 &= \partial_y(T_1 - S_1) + \partial_z^4 \psi_1, \\ 0 &= \partial_z^2 T_1, \\ 0 &= \partial_z^2 S_1. \end{aligned}\right\} \tag{3.5}$$

The fixed-temperature boundary condition determines the first-order temperature field, while the salinity is undetermined at this order. Thus the solution of (3.5) is

$$T_1 = a_1\theta(y), \quad S_1 = S_1(y, t_2), \quad \psi_1 = W(z)\partial_y(S_1 - a_1\theta). \tag{3.6 a–c}$$

Because the boundary conditions on the salinity field only determine its flux, the depth-averaged salinity can be much larger than might be anticipated by naive scaling arguments. In this case the surface salinity flux is $O(\epsilon^3)$, yet the depth-average salinity field, S_1, is $O(\epsilon)$ and its evolution is determined at third order.

The shape function $W(z)$ depends on the boundary conditions on ψ at $z = 0$ and 1. For no-stress one finds

$$W(z) \equiv \tfrac{1}{24}(z^4 - 2z^3 + z). \tag{3.7}$$

Other boundary conditions lead to different quartic polynomials but, in anticipation of our results below, there are no qualitative effects introduced by different homogeneous boundary conditions on ψ.

The smallness of the aspect ratio, ϵ, together with the restriction to small thermal and saline Rayleigh numbers (3.2), forces vertical diffusion to dominate. As a consequence, the lowest-order salinity and temperature fields are vertically homogeneous. Of course, in the ocean the Rayleigh numbers are very large, advection overwhelms mixing and the temperature and salinity are stratified. However, the scaling (3.2) permits analytic progress and despite the unrealistic vertical structures of the fields, we will show that it leads to multiple equilibria.

3.2. *The second-order solution*

At next order, ϵ^2, one has:

$$P^{-1}J(\psi_1, \partial_z^2\psi_1) = \partial_y(T_2 - S_2) + \partial_z^4\psi_2, \tag{3.8a}$$

$$-\partial_z\psi_1\partial_y T_1 = \partial_z^2 T_2, \tag{3.8b}$$

$$-L^{-1}\partial_z\psi_1\partial_y S_1 = \partial_z^2 S_2. \tag{3.8c}$$

The temperature and salinity equations can be integrated in z:

$$-\psi_1\partial_y T_1 = \partial_z T_2, \tag{3.9a}$$

$$-L^{-1}\psi_1\partial_y S_1 = \partial_z S_2. \tag{3.9b}$$

Note that $\partial_z S_2 = 0$ at both boundaries so the boundary conditions on salinity are automatically satisfied at this order. (Because $b \sim \epsilon^3$ the imposed salinity flux does not enter till third order.) Thus at second order there is no solvability condition to determine $S_1(y, t_2)$.

One can now integrate (3.9) to obtain explicit expressions for S_2 and T_2. With the polynomial $W(z)$ in (3.7) one finds

$$\left.\begin{aligned} T_2 &= -a_1\,\partial_y\theta(\partial_y S_1 - a_1\,\partial_y\theta)\,U(z), \\ S_2 &= -L^{-1}\partial_y S_1(\partial_y S_1 - a_1\,\partial_y\theta)\,[U(z)+\tfrac{1}{240}], \end{aligned}\right\} \tag{3.10}$$

where the shape function $U(z)$ is

$$U(z) = \tfrac{1}{240}(2z^5 - 5z^4 + 5z^2 - 2). \tag{3.11}$$

The constants of integration in (3.10) are determined imposing the boundary conditions $T_2(y,1) = \partial_z T_2(y,0) = \partial_z S_2(y,0) = 0$ and requiring that the vertical average of S_2 vanishes. This second condition amounts to a definition of $S_1(y,t_2)$ as the vertically averaged salinity. We do not need the explicit expression for ψ_2 (the shape function is a ninth-order polynomial), but if necessary it could be calculated by four integrations of (3.8a).

Finally, we observe that there is no heat flux through the top boundary due to either T_1 or T_2 (from (3.9) $\partial_z T_2 = 0$ at $z = 1$). At third order we find a non-zero heat flux, and of course it is at third order that a non-zero saline flux first appears. Thus, despite the superficial disparity implied by the scaling in (3.2), the thermal and saline fluxes are actually of the same order, i.e. ϵ^3.

3.3. *The third-order solution and the solvability condition*

The salinity equation at $O(\epsilon^3)$ is

$$L^{-1}[\partial_{t_2} S_1 + J(\psi_1, S_2) - \partial_z\psi_2\,\partial_y S_1] = \partial_z^2 S_3 + \partial_y^2 S_1. \tag{3.12}$$

At this order the salinity field is forced by the imposed flux, $\partial_z S_3(1,y) = b_3 F(y)$. The solvability condition is obtained integrating (3.12) vertically:

$$L^{-1}\left[\partial_{t_2} S_1 + \partial_y \int_0^1 \psi_1\,\partial_z S_2\,\mathrm{d}z\right] = b_3 F(y) + \partial_y^2 S_1. \tag{3.13}$$

Substituting the expression (3.6c) for ψ_1 and (3.9b) for $\partial_z S_2$ into (3.13) we find the evolution equation for the vertically averaged salinity field

$$L^{-1}\partial_{t_2} S_1 - L^{-2}\left[\int_0^1 W^2(z)\,\mathrm{d}z\right]\partial_y(\partial_y S_1(\partial_y S_1 - a_1\,\partial_y\theta)^2) = b_3 F(y) + \partial_y^2 S_1. \tag{3.14}$$

3.4. *The canonical form of the amplitude equation*

We now put the amplitude equation (3.14) in canonical form using a cosmetic rescaling. We introduce a new time

$$\tau \equiv L t_2 = \frac{\pi^2 \kappa_S}{l^2} t, \tag{3.15}$$

where t in (3.15) is the dimensional time variable. We define a new independent variable

$$\sigma(y,\tau) \equiv a_1^{-1} S_1, \tag{3.16}$$

and then (3.14) is

$$\partial_\tau \sigma - \mu^2\,\partial_y[\partial_y\sigma(\partial_y\sigma - \partial_y\theta)^2] = rF(y) + \partial_y^2\sigma - \gamma^2\,\partial_y^4\sigma, \tag{3.17}$$

where the coefficients are

$$\mu^2 \equiv L^{-2}a_1^2\int_0^1 W^2(z)\,\mathrm{d}z, \quad r \equiv \frac{b_3}{a_1}. \tag{3.18}$$

With the polynomial $W(z)$ in (3.7) the integral in (3.18) is $\int W^2(z)\,\mathrm{d}z = 1/19040$.

In (3.17) we have also added a fourth-order hyperdiffusion term, $\gamma^2 \partial_y^4 \sigma$, to 'regularize' the equation. We show below that without this term the amplitude equation develops discontinuities in $\partial_y \sigma$. The hyperdiffusion smooths these jumps by forming boundary layers of thicknesses γ. Apart from this, the role of γ is limited and provided it is small it does not effect the qualitative properties of the solution. For instance, both the location and the size of the jumps in σ_y are independent of γ.

A further justification for the *ad hoc* introduction of the hyperdiffusion is that we anticipate the arrival of a term with this form at fifth order in the ϵ expansion. In particular, the 'cross-term' $\partial_y^2 \partial_z^2 \psi$ in the vorticity equation eventually generates a term proportional to $\partial_y^4 S_1$ in the vertically averaged salinity balance at ϵ^5. The reconstituted amplitude equation then contains $\gamma^2 \partial_y^4 \sigma$ with $\gamma \sim \epsilon$.

The boundary conditions on (3.17) are

$$\partial_y \sigma(\pm\pi, \tau) = 0, \quad \partial_y^3 \sigma(\pm\pi, \tau) = 0, \tag{3.19}$$

and they are obtained enforcing no salt flux and no stress at the lateral boundaries. (We are implicitly assuming that $\partial_y \theta(\pm\pi) = \partial_y^3 \theta(\pm\pi) = 0$).

Equation (3.17) is the canonical form of the amplitude equation. Although the original equations contained five non-dimensional parameters, the reduced system in (3.17) contains three: r, μ and γ. And we show below that γ has no qualitative importance: it is r and μ which determine the structure of multiple solutions.

3.5. *A discussion of the physical basis of the expansion*

The non-dimensional amplitude equation in (3.17) is an equation for the vertically averaged salinity:

$$\bar{S}(y, t) \equiv \frac{1}{d} \int_0^d S(y, z, t)\, \mathrm{d}z. \tag{3.20}$$

In (3.20) we use the dimensional variables introduced at the beginning of § 2. In terms of these dimensional variables the amplitude equation (3.17) is

$$\partial_t \bar{S} = \kappa_S \partial_y^2 \bar{S} + c \frac{d^8 g^2}{\nu^2 \kappa_S} \partial_y [(\alpha_S \partial_y \bar{S} - \alpha_T \partial_y \bar{T})^2 \partial_y \bar{S}] + \frac{\kappa_S \Delta S}{d^2} F(y). \tag{3.21}$$

where c is a dimensionless constant whose value depends on the boundary conditions used for ψ. Equation (3.21) is a nonlinear diffusion equation for the vertically averaged salinity field in (3.20). The nonlinear part of the diffusivity increases with the square of the density gradient, $\alpha_S \partial_y \bar{S} - \alpha_T \partial_y \bar{T}$.

The asymmetry between T and S is evident. It is not necessary to find a conservation equation for $\bar{T}$, analogous to (3.21), because the fixed temperature condition at the upper boundary ensures that $\bar{T} \approx \Delta T \theta(y)$. The fixed flux condition on salinity is not so constraining.

The expansion which leads to (3.21) has several unrealistic restrictions which should be noted. Equation (3.6*a*, *b*) shows that the leading terms in both the temperature and salinity fields are independent of z. Thus the whole expansion springs from using (3.2) to restrict the amplitude of the thermal and saline forcing so that vertical diffusion of temperature and salinity is faster than the generation of vertical inhomogeneities by differential horizontal advection. This assumption is identical to the approximation in Taylor's (1953) discussion of shear dispersion, viz. because v depends on z the term $v \partial_y \bar{S}$ in (2.1*e*) continuously creates depth dependent salinity variations from the depth-averaged field. This creation is balanced by vertical diffusion, as shown in (3.8*b*) and (3.8*c*).

The salinity and temperature fields in the ocean are not uniform in the vertical to even a rough approximation. Although the aspect ratio, ϵ, is of order $\frac{1}{1000}$ the thermal and saline Rayleigh numbers are so large that the velocities overwhelm the vertical mixing.

However, the calculations by Thual & McWilliams (1991, figure 2) show that the temperature and salinity are not far from being vertically homogeneous. In §5 we argue that (3.21) does capture the essential structure of the multiple equilibria reported by Thual & McWilliams. As yet there is no evidence that either general circulation models or multi-box models have multiple equilibria which differ qualitatively from the examples described by Thual & McWilliams and by us in §5.

4. Variational structure of the amplitude equation

Some general properties of the amplitude equation are revealed by considering the evolution equation in terms of the salinity gradient, $\chi \equiv \partial_y \sigma$, and the temperature gradient, $\eta \equiv \partial_y \theta$. Taking the y-derivative of (3.17) we have

$$\partial_\tau \chi = \partial_y^2 [\mu^2 \chi(\chi-\eta)^2 - rf(y) + \chi - \gamma^2 \partial_y^2 \chi], \tag{4.1}$$

where we have introduced

$$f(y) \equiv -\int_{-\pi}^{y} F(y_1)\, \mathrm{d}y_1. \tag{4.2}$$

Notice that $f(\pi)$ must vanish in order for the net salinity flux into the domain to be zero. We assume that this is the case. The boundary conditions in (3.18) translate to $\chi = \partial_y^2 \chi = 0$ at $y = \pm\pi$.

Equation (4.1) is the Cahn–Hilliard (1958) equation with non-constant coefficients. A recent review of its mathematical properties (for constant coefficients) can be found in Alikakos, Bates & Fusco (1991). Equation (4.1) can be written as

$$\partial_\tau \chi = \partial_y^2 \frac{\delta \Phi}{\delta \chi}, \tag{4.3}$$

where $\Phi[\chi]$ is the functional

$$\Phi[\chi] \equiv \int_{-\pi}^{\pi} [V(\chi, y) + \tfrac{1}{2}\gamma^2 (\partial_y \chi)^2]\, \mathrm{d}y, \tag{4.4}$$

and $V(\chi, y)$ is the function

$$V(\chi, y) \equiv \mu^2 (\tfrac{1}{4}\chi^4 - \tfrac{2}{3}\chi^3 \eta) + \tfrac{1}{2}\chi^2 (1 + \mu^2 \eta^2) - r f \chi. \tag{4.5}$$

In (4.3) we have introduced the variational derivative of the functional $\Phi[\chi]$:

$$\frac{\delta \Phi}{\delta \chi} = V_\chi - \gamma^2 \partial_y^2 \chi. \tag{4.6}$$

The advantage of the form (4.3) is that one can now show by direct calculation that Φ is a Lyapunov functional. Specifically:

$$\begin{aligned} \partial_\tau \Phi &= \int_{-\pi}^{\pi} \chi_\tau \frac{\delta \Phi}{\delta \chi} \mathrm{d}y, \\ &= -\int_{-\pi}^{\pi} \left(\partial_y \frac{\delta \Phi}{\delta \chi} \right)^2 \mathrm{d}y < 0. \end{aligned} \tag{4.7}$$

Because Φ is bounded from below and always decreases in time, a steady state must be reached where Φ is local minimum. The integral result (4.7) guarantees that the system has at least one stable equilibrium which minimizes the Lyapunov functional Φ.

We now proceed to analyse the steady solutions of (4.1). The stability of these solutions can be assessed by calculating $\Phi[\chi]$ and determining which steady solution minimizes this functional. The linearly stable steady solutions are local minima and unstable steady solutions are local maxima or saddle points of $\Phi[\chi]$.

4.1. *Steady solutions and their stability*

The steady state solutions of (4.1) satisfy

$$\frac{\delta\Phi}{\delta\chi} = \mu^2\chi(\chi-\eta)^2+\chi-rf-\gamma^2\partial_y^2\chi = 0, \tag{4.8}$$

with $\chi(\pm\pi) = 0$. Because γ is a small number, the term $\gamma^2\partial_y^2\chi$ can be neglected except in boundary-layer regions. Thus outside of boundary layers the steady solutions are obtained approximately by solving the cubic algebraic equation

$$V_\chi = \mu^2\chi(\chi-\eta)^2+\chi-rf = 0, \tag{4.9}$$

for the salinity gradient, χ, as a function of y.

The cubic equation in (4.9) sometimes has three real solutions, but depending on the values of the parameters μ and r and the position y, there may only be one. Consider, for example, θ and F to be symmetric functions of y. Thus η and f are antisymmetric functions which both vanish at the equator $y = 0$. It is clear from inspection of (4.9) that at $y = 0$ there is only one real solution, namely $\chi(0) = 0$. On the other hand, there might be locations where the cubic has three real solutions. To illustrate this possibility concretely consider the special case in which $rf(y) = \eta(y)$, so that the cubic in (4.9) can be factorized conveniently. The three roots are then

$$\left.\begin{aligned}\chi_A(y) &= \tfrac{1}{2}\eta+(\tfrac{1}{4}\eta^2-\mu^{-2})^{\frac{1}{2}},\\ \chi_B(y) &= \tfrac{1}{2}\eta-(\tfrac{1}{4}\eta^2-\mu^{-2})^{\frac{1}{2}},\\ \chi_C(y) &= \eta.\end{aligned}\right\} \tag{4.10}$$

Thus in those regions where η exceeds $2/\mu$, χ can take any of the three possible values which are the extrema of $V(\chi)$. Only χ_A and χ_C in (4.10) are local minima of $V(\chi)$. The third solution branch, χ_B is a maximum and, as one expects from the earlier variational arguments, this branch is unstable to infinitesimal perturbations. A proof is given in Appendix A.

In figure 1 we plot the cubic polynomial V_χ and show a convenient geometric argument (the 'Maxwell construction') which determines the relative values of V at the three equilibrium points. Referring to figure 1

$$V(\chi_B) = V(\chi_A)+P, \quad V(\chi_C) = V(\chi_B)+Q, \tag{4.11}$$

where P and Q are the areas under the curve V_χ. Q is negative because it lies below the χ-axis. Thus $V(\chi_B) > V(\chi_A)$ and $V(\chi_B) > V(\chi_C)$, i.e. $V(\chi_B)$ is a local maximum. It is also clear in figure 1 that $P > |Q|$ so $V(\chi_C) = V(\chi_A)+P+Q > V(\chi_A)$, i.e. $V(\chi_A)$ is the global minimum of $V(\chi)$. Hence to construct a steady, linearly stable solution we can select either of the solution branches $\chi_A(y)$ or $\chi_C(y)$.

A linearly stable solution might be constructed by selecting the local minimum, $\chi_C(y)$, but because $V(\chi_A) < V(\chi_C)$ this solution is unstable to strong perturbations.

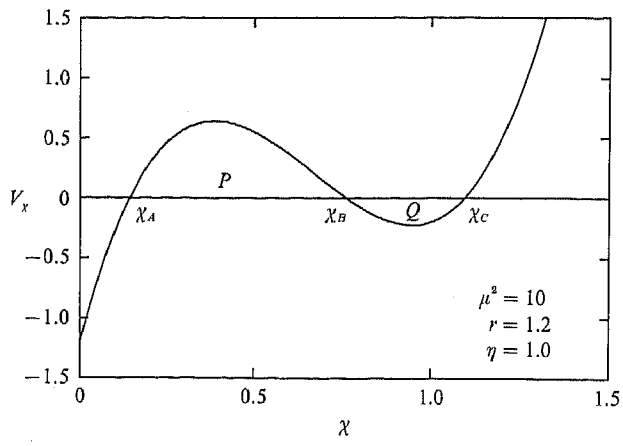

FIGURE 1. The cubic polynomial V_χ in (4.9) with $\mu^2 = 10$, $r = 1.2$ and $\eta = 1$. The three zeros correspond to the three solution branches. In this case, because the area P is bigger than the area Q, we have $V(\chi_B) > V(\chi_C) > V(\chi_A)$. The areas P and Q are equal when the inflexion point of V_χ, i.e. the point where $V_{\chi\chi\chi} = 0$, coincides with χ_B.

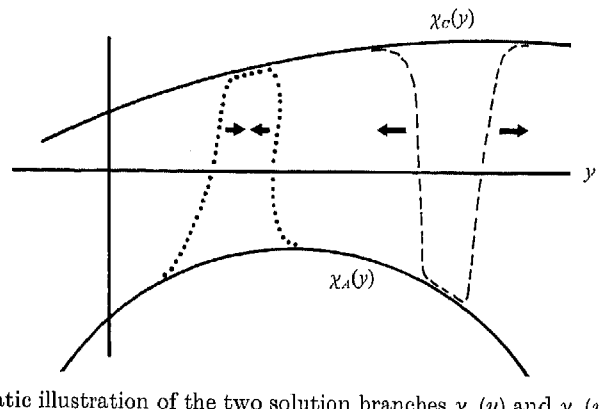

FIGURE 2. A schematic illustration of the two solution branches $\chi_A(y)$ and $\chi_C(y)$. As in figure 1 we suppose that $V(\chi_C) > V(\chi_A)$. Because both χ_A and χ_C are local minima both of these branches are linearly stable, but because χ_A is the global minimum a large localized perturbation of χ_C, such as the dashed curve, can expand so that χ_A replaces χ_C. By contrast a large localized perturbation of χ_A, such as the dotted curve, shrinks and leaves χ_A.

For instance if we perturb $\chi_C(y)$ in a small region by jumping to the $\chi_A(y)$ branch and back again (see figure 2) then this 'bubble' grows so that $\chi_A(y)$ replaces $\chi_C(y)$ in all of the contiguous region where $V(\chi_A) < V(\chi_C)$. Thus the branch $\chi_C(y)$ is 'metastable'.

Alternatively one can construct a solution by selecting the global minimum, $\chi_A(y)$. This solution is not only linearly stable, but it also resists strong perturbations, i.e. 'bubbles' of $\chi_C(y)$ shrink as they are replaced by $\chi_A(y)$.

4.2. *Changes of solution branch at critical points*

There are particular values of y at which $V(\chi_A) = V(\chi_C)$, i.e. the areas P and Q in figure 1 are equal in magnitude. We refer to these positions, at which an exchange of global minima between branches occurs, as critical points.

For instance, if $rf(y) = \eta(y)$, as we assumed in (4.10), then one can show that the location of the critical points, denoted by y_S, is determined by solving

$\eta^2(y_S) = 9/(2\mu^2)$. This condition ensures that the inflexion point of the cubic V_χ, which is at $\chi = \frac{2}{3}\eta$, coincides with χ_B. Then from symmetry the two areas P and Q in figure 1 are equal.

The critical points are significant landmarks on the y-axis because, at these points, (4.8) has steady solutions which jump between branches. The jump is accomplished in a boundary layer of thickens γ, so that $\gamma^2\chi_{yy}$ in (4.8) is of order unity in the neighbourhood of y_S. Further details of the boundary-layer solution are in Appendix B. Here we give a simple proof that steady boundary-layer solutions are only possible at the critical points.

Multiplying (4.8) by χ_y and integrating across the boundary layer at y_S one finds that

$$[\tfrac{1}{2}\gamma^2\chi_y^2 - V(\chi)]_{y_S-\infty}^{y_S+\infty} = 0. \tag{4.12}$$

Since the term $\frac{1}{2}\gamma^2\chi_y^2$ is very small on either side of the boundary layer (i.e. at $y = y_S \pm \infty$) we see from (4.12) that $V(\chi)$ must not jump when χ changes branch in a boundary layer at y_S.

To summarize, steady boundary-layer solutions which pass from one solutions branch to another are only possible at critical points where $V(\chi_A) = V(\chi_C)$. $\chi(y)$ jumps as one passes through one side of the boundary layer at y_S to the other. $V(\chi)$ does not jump as one passes through the boundary layer. Using the geometry in figure 1, the critical points are located by requiring that the two areas P and Q are equal in magnitude.

5. Multiple equilibria in the example of Thual & McWilliams

Thual & McWilliams (1991) solved the full equations of motion in (2.4) using a numerical scheme. Their forcing functions were

$$\theta(y) = F(y) = \cos y, \quad \eta(y) = f(y) = -\sin y. \tag{5.1}$$

These forms correspond to a surface temperature condition with a warm equator ($y = 0$) and cold polar regions ($y = \pm\pi$). The surface boundary condition for salt imposes positive flux into the ocean at the equator (evaporation exceeds precipitation) and negative flux at the poles (precipitation exceeds evaporation).

In this section we illustrate the abstract arguments of §4 by solving (4.8) with $\eta(y)$ and $f(y)$ in (5.1). With these choices the steady form of the amplitude equation in (4.8) is

$$\mu^2\chi(\chi + \sin y)^2 + \chi + r\sin y = \gamma^2\,\partial_y^2\chi. \tag{5.2}$$

As explained in §4, we suppose that $\gamma \ll 1$ and find approximate solutions by solving the cubic polynomial obtained by neglecting the right-hand side of (5.2), i.e. $V_\chi = \mu^2\chi(\chi+\sin y)^2 + \chi + r\sin y = 0$. We anticipate changes of branch and boundary layers of thickness γ at the critical points.

5.1. *Two limiting cases: large and small r*

For large r there is a single real solution of (5.2) given approximately by the dominant balance $\mu^2\chi^3 \approx -r\sin y$ in (5.2). The results of a numerical solution of $V_\chi = 0$ with $r = 2$ and $\mu^2 = 10$ are plotted in figure 3(*a*). This solution is salinity dominated because water sinks at the equator and upwells at the poles. (Notice that in the present notation the leading-order streamfunction in (3.6*c*) is proportional to the density gradient, $\chi - \eta$, and that $W(z)$ in (3.7) is positive definite. The dashed line in figure 3(*a*) shows that $w = \psi_y \sim \chi_y - \eta_y$ is positive at $y = \pm\pi$.)

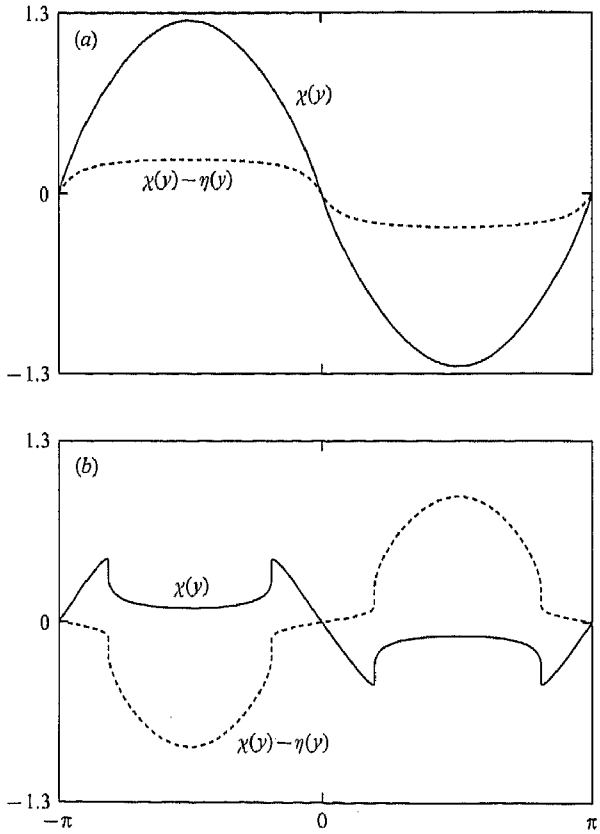

FIGURE 3. (a) ———, Only real solution of $V_\chi = 0$ when $\mu^2 = 10$ and $r = 2$; – – –, total density gradient, $\chi - \eta$. Because the sign of the density gradient is the same as the sign of the salinity gradient, $\chi(y)$, we refer to this as 'salinity dominated flow'. We explain in the text that this implies that fluid upwells at the poles and sinks at the equator. (b) ———, Only real solution of $V_\chi = 0$ when $\mu^2 = 10$ and $r = 0.9$; – – –, total density gradient, $\chi - \eta$. Because the sign of the density gradient is the same as the sign of the temperature gradient, $\eta(y) = -\sin y$, we refer to this as 'thermally dominated flow'. The circulation in this case sinks at the poles and upwells at the equator.

At the other end of the parameter space, for small r, the thermal forcing dominates and the water sinks at the poles. Again, there is only one real solution of (5.2). The dominant balance is $(\mu^2 \sin^2 y + 1)\,\chi \approx -r \sin y$ and the results of a numerical solution with $r = 0.9$ and $\mu^2 = 10$ are plotted in figure 3(b).

5.2. *Intermediate values of r*

The cubic polynomial, $V_\chi = 0$, has three real solutions when r is of order unity. But, as figure 4(a) shows, these three solution branches exist only in a part of the domain $-\pi < y < \pi$. For instance, if we start at $y = -\pi$ and move north then at first there is only one solution branch available, namely $\chi_C(y) \approx -r \sin y$. This is the saline branch because the sign of the density gradient is the same as the sign of the salinity gradient (this is not shown in figure 4). But at $y = -(\frac{1}{2}\pi) - \lambda$ the other two solution branches appear and continue till $y = -(\frac{1}{2}\pi) + \lambda$. Then in the equatorial band, $-(\frac{1}{2}\pi) + \lambda < y < (\frac{1}{2}\pi) - \lambda$, there is again only one solution available. The northern hemisphere is simply an antisymmetric reflection of the southern. Thus there are two 'midlatitude' bands where multiple solution branches exist. There is the southern band, $-\frac{1}{2}\pi - \lambda < y < -\frac{1}{2}\pi + \lambda$, and the northern band, $\frac{1}{2}\pi - \lambda < y < \frac{1}{2}\pi + \lambda$.

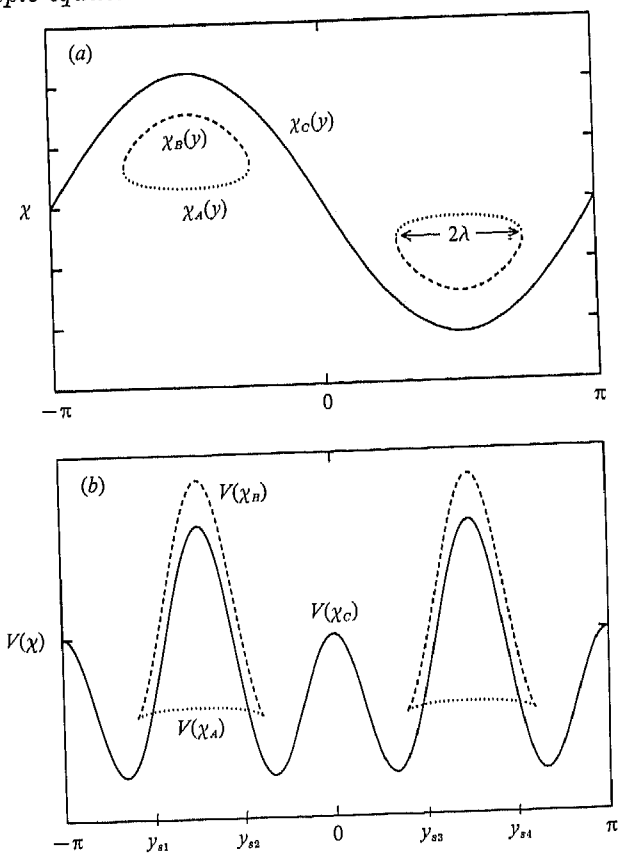

FIGURE 4. (*a*) This shows the three real solutions of $V_\chi = 0$ when $\mu^2 = 10$ and $r = 1.2$ as functions of y. There is only one branch, $\chi_C(y)$ which exists for all y. Multiple equilibria are possible because the solution can jump from $\chi_C(y)$ to $\chi_A(y)$ in the midlatitude bands where three real solution branches exist. (Jumps to $\chi_B(y)$ are possible, but these correspond to linearly unstable solutions.) (*b*) This shows the potential, $V(\chi)$, evaluated at the three solution branches from part (*a*). The critical points at which $V(\chi_C(y)) = V(\chi_A(y))$ are indicated by y_{S1}–y_{S4}. At these points one can construct boundary-layer solutions which jump between χ_C and χ_A.

Analytic expressions for λ as a function of r and μ^2 are complicated, and not informative. More important landmarks are the locations, y_S, of the critical points. These are the solutions of

$$(\sin y_S)^2 = 9\mu^{-2}(\tfrac{3}{2}r - 1). \tag{5.3}$$

(This result is derived in Appendix B.) Notice that the four solutions of (5.3) (denoted by y_{S1} to y_{S4} and shown in figure 4*b*) do not coincide with the four locations at which multiple solutions appear and disappear (i.e. $y = \pm(\frac{1}{2}\pi) \pm \lambda$). The critical points lie properly within the midlatitude multiple solutions bands.

To construct a steady stable solution, one begins at $y = -\pi$ on the only available solution branch of (5.2) (the saline branch, denoted by $\chi_C(y)$ in figure 4*a*) and moves northward past $-(\frac{1}{2}\pi) - \lambda$. At the first critical point, y_{S1}, one has a choice. It is possible to stay on the saline branch, $\chi_C(y)$, and continue northward. The alternative is to jump at y_{S1} to the thermal branch, $\chi_A(y)$, and then jump back to $\chi_C(y)$ at y_{S2}. In the interval $y_{S1} < y < y_{S2}$ it turns out that $V(\chi_A) < V(\chi_C)$ so the first alternative, χ_C, is a metastable solution, while the second, χ_A, is stable even to large perturbations. In the northern hemisphere one is presented with the same choice at y_{S2}.

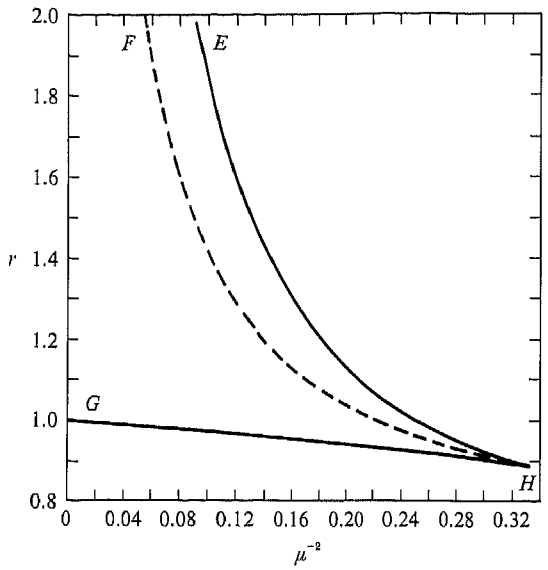

FIGURE 5. The (μ^{-2}, r) parameter plane. The cubic polynomial $V_\chi = 0$ has three real roots inside the region EHG. However, the differential equation (5.2) has multiple solutions only within FHG. The cusp, H, is at $r = \frac{8}{9}$ and $\mu^2 = 3$.

To summarize, there is a choice (to jump or not to jump) in each hemisphere, and so there are four different linearly stable solutions. Three of these are metastable because a large localized salinity perturbation of the saline branch, $\chi_C(y)$, can punch through to the thermal branch, $\chi_A(y)$, and expand because $V(\chi_A) < V(\chi_c)$ (figure 4*b*). Two of the three metastable solutions are asymmetric about the equator because there is a jump in only one hemisphere. The other metastable solution, which has no jumps, is just the saline branch $\chi_C(y)$, and so is symmetric. The fourth, nonlinearly stable solution is a global minimum of $V(\chi)$. It has a jump to the thermal branch in both hemispheres and so is symmetric about the equator.

The discussion in the previous paragraphs has referred to figure 4 in which $r = 1.2 > 1$. Analogous multiple solutions exist when $r < 1$, but in this case the branch $\chi_C(y)$, which exists for all $-\pi < y < \pi$, is a thermal flow with sinking at the poles and upwelling at the equator. At the transition, $r = 1$, the branch $\chi_C(y)$ is given by (4.10*c*), so that there is no density gradient ($\chi - \eta = 0$) and therefore no motion ($\psi_1 = \psi_2 = 0$).

5.3. *The domain of existence and stability of multiple states*

Multiple solutions of the cubic polynomial on the left-hand side of (5.2) can only be found if

$$|27r - 18 - 2\mu^2| \leqslant 2\mu^2(1 - 3\mu^{-2})^{\frac{3}{2}}. \tag{5.4}$$

(This result is obtained using the formula for the solution of a cubic polynomial.) The boundary of this domain is shown in figure 5 by the solid curve EHG. There is a cusp at the point H which is at $r = \frac{8}{9}$ and $\mu^2 = 3$.

However, only a subset of the domain defined by (5.4) supports stable multiple equilibria. Analysis of the function $V(\chi)$ reveals that for

$$27r - 18 - 2\mu^2 \geqslant 0, \tag{5.5}$$

(the dashed curve FH) only one symmetric state can be constructed. A representative

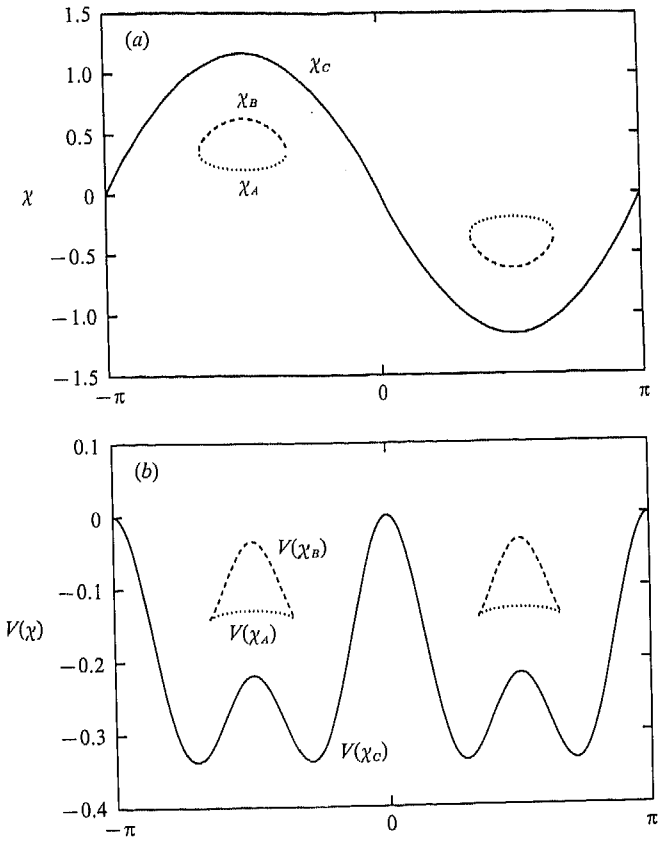

FIGURE 6. (*a*) The real solutions of $V_\chi = 0$ when $\mu^2 = 10$ and $r = 1.5$. This point is within the region *EHF* in figure 5. As in figure 4, there is midlatitude band in which this cubic has three real solutions. (*b*) The potential, $V(\chi)$, evaluated at the three solution branches from (*a*). There are no critical points at which changes of branch can occur. We conclude that multiple solutions of the differential equation (5.2) are not possible within *EHF*.

solution with parameters in the region *EHF* is shown in figure 6. Notice that $V(\chi_A)$, shown as a dotted line in figure 6 (*b*), is always larger than $V(\chi_C)$, shown as a solid line. Therefore within *EHF* thee is no critical point at which χ_C can jump to χ_A *via* an internal boundary layer.

To summarize, multiple solutions of the differential equation (5.2) (such as that shown in figure 4) are found within the domain *FHG*. The lower curve, *GH*, is given by $27r-18-2\mu^2 = -2\mu^2(1-3\mu^{-2})^{\frac{3}{2}}$ and the upper curve, *FH*, by $27r-18-2\mu^2 = 0$. The two curves meet in a cusp at $r = \frac{8}{9}$ and $\mu^2 = 3$.

5.4. *Comparison with the numerical solution*

Thual & McWilliams (1991) solved the unreduced equations of motion in (2.8) numerically. In a control space analogous to that in figure 5 they found two cusp catastrophes. Based on calculations with $\epsilon = 1$ and $\epsilon = 0.4$ they concluded that as $\epsilon \to 0$ the two cusps merge and both converge to $(a, b) = (\epsilon a_1, \epsilon^3 b_3) = (0, 0)$. The amplitude expansion used here supports both of these conclusions: we find only one cusp catastrophe and, since a_1 and b_3 are fixed as $\epsilon \to 0$, this point converges to $(a, b) = (0, 0)$ as $\epsilon \to 0$.

Thual & McWilliams also speculated that as $\epsilon \to 0$ the cusps approach the 'zero

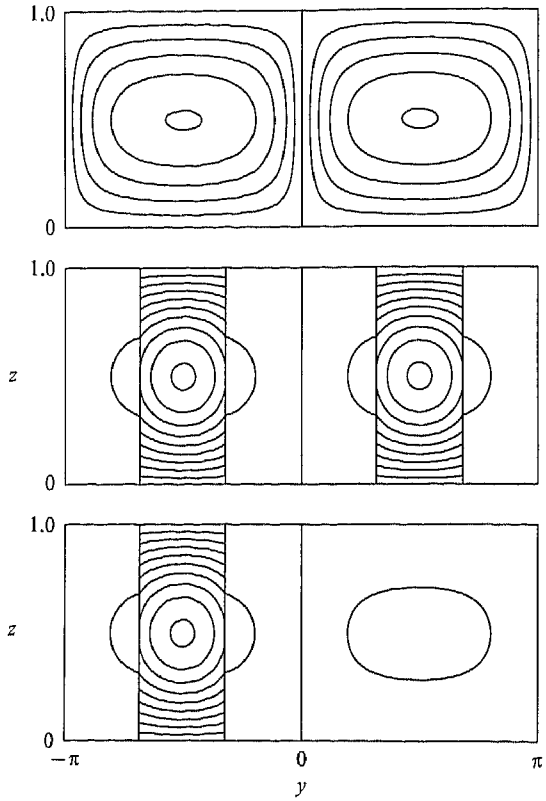

FIGURE 7. This figure shows the leading-order approximation to the streamfunction,

$$\psi_0 \sim (\chi(y)-\eta(y))\, W(z),$$

for three of the four linearly stable solutions in figure 4. We have not included the boundary-layer corrections (Appendix B) so that the streamfunctions shown in this figure are discontinuous at the critical points. (*a*) This shows the saline mode in which $\chi = \chi_C$ everywhere. There are no changes of branch. This flow is symmetric about the equator and is metastable. (*b*) This shows the thermal flow in which χ jumps from χ_C to χ_A and back in both hemispheres. The flow is symmetric about the equator. (*c*) This shows one of the two asymmetric solutions. In this case there is a jump in the southern hemisphere, but not in the northern hemisphere. (The other asymmetric solution is a reflection of this one.)

circulation line'. In our terminology this is $r = 1$. (Note that when $r = 1$ the cubic polynomial on the left-hand side of (5.2) has a root $\chi_C(y) = \eta(y)$ which corresponds to no density gradient and no motion.) Our results disagree with this conclusion: the cusp in figure 5 is at $r = \frac{8}{9}$, not $r = 1$. It may be that the numerical calculations with $\epsilon = 0.4$ were not close enough to asymptotic values to distinguish between 1 and $\frac{8}{9}$.

A second point of disagreement between the amplitude equation and the full numerical solution is indicated in figure 7. In his figure we contour the leading-order approximation to the stream function

$$\psi_1(y,z) = a_1(\chi-\eta)\, W(z) \tag{5.6}$$

for three of the four multiple solutions shown in figure 4. (We show only one of the two asymmetric states, since the other is merely a reflection of the first.) The asymmetric flow in figure 7(*c*) jumps to the thermal branch in the southern hemisphere, but not in the northern hemisphere. Since both χ and η are zero at $y = 0$

the equatorial line, $y = 0$, is a streamline separating the strong thermal cell in the southern hemisphere from the weaker saline cell in the northern hemisphere. Note that both cells circulate in the same direction.

The results in Thual & McWilliams (1991) show that the asymmetric circulation actually consists of a single pole-to-pole cell. Their figure 2(*c*) shows that in the asymmetric solution the stream function is much larger in one hemisphere than in the other but, in contrast to figure 7(*c*) the equatorial line is not a streamline separating two cells. This failure of the amplitude equation might be corrected by the inclusion of higher-order terms in ϵ.

6. Conclusion

In this article we have used an expansion in aspect ratio to simplify the two-dimensional non-rotating thermohaline convection equations in (2.1). The result of the expansion is the equation (3.21) for the vertically averaged salinity field. The asymmetry between temperature and salinity arises from the different boundary conditions. At the top of the domain the temperature and the salinity flux are prescribed.

The expansion we have used has some unrealistic limitations described in the discussion below (3.21). Despite these limitations (3.21) has several advantages over the increasingly elaborate box models which have been advanced as attempts to make the original Stommel (1961) two-box model more realistic. First, (3.21) is a rational approximation to the dynamics of non-rotating two-dimensional thermohaline convection in (2.1) and could be compared quantitatively and systematically with numerical solutions of that system. The same cannot be said for multi-box models. Further, it is possible to extend (3.21) to include three dimensions and rotation.

The second advantage of (3.21) is that it is more compact and more analytically tractable than multi-box models. In support of this assertion we emphasize the utility of the variational formulation in §4. With the variational principle we can construct the steady solutions by identifying the points at which changes of branch occur (the critical points) and we also have a succinct characterization of their stability. This allows us to distinguish between steady solutions which are local minima and those which are global minima. The local minima are linearly stable, but are vulnerable to large spatially localized perturbations. On the other hand, the global minimum resists even large perturbations. The difference is illustrated schematically in figure 2.

It is interesting that in the example discussed in §5 the multiple branches occur only in a midlatitude band (see figure 4). This means that the local minima are most vulnerable to perturbations in this midlatitude region. For instance, the saline branch, $\chi_C(y)$, in figure 4(*a*) can be destabilized by a localized salinity perturbation only in the region where the alternative steady solutions exist. In the equatorial and polar regions it should be resistant to even large-amplitude perturbations. It would be interesting to see if the multiple equilibria in general circulation models, such as that of Bryan (1886), are selectively sensitive to midlatitude perturbations.

We are supported by grants from the Oceanography Division of the National Science Foundation. We thank Lisa Stockinger for her help with the computations reported here. The impetus for this research originated at the 1991 Woods Hole Summer Program in Geophysical Fluid Dynamics. We thank Henry Stommel for

interesting us in the general question of multiple thermohaline equilibria, and Stephan Fauve for introducing us to the variational methods used in this article.

Appendix A. Linear stability near a stationary solution

The evolution equation can be written in the form

$$\partial_\tau \chi = \partial_y^2\left(\frac{\delta \Phi}{\delta \chi}\right), \tag{A 1}$$

with the Lyapunov functional, $\Phi(\chi)$, defined in (4.4). A stationary solution, χ_0 satisfies

$$\left.\frac{\delta \Phi}{\delta \chi}\right|_{\chi_0} = 0, \tag{A 2}$$

and in the vicinity of the stationary solution the functional derivative of Φ can be approximated by

$$\frac{\delta \Phi(\chi)}{\delta \chi} = (\chi-\chi_0)\left.\frac{\delta^2 \Phi}{\delta \chi^2}\right|_{\chi_0} + O((\chi-\chi_0)^2). \tag{A 3}$$

The linear stability problem is then

$$\partial_\tau (\chi-\chi_0) = \partial_y^2\left[(\chi-\chi_0)\left.\frac{\delta^2 \Phi}{\delta \chi^2}\right|_{\chi_0}\right]. \tag{A 4}$$

Multiplying (A 4) by the quantity inside the square brackets and integrating over the domain one has

$$\partial_\tau \int_{-\pi}^{\pi} (\chi-\chi_0)^2 \left.\frac{\delta^2 \Phi}{\delta \chi^2}\right|_{\chi_0} \mathrm{d}y = -2\int_{-\pi}^{\pi}\left[\partial_y (\chi-\chi_0)\left.\frac{\delta^2 \Phi}{\delta \chi^2}\right|_{\chi_0}\right]^2 \mathrm{d}y. \tag{A 5}$$

The right-hand side of (A 5) is positive definite, while the sign of the left-hand side depends on the curvature of the Lyapunov functional at the extremum location, χ_0. If the stationary solution, χ_0, is a minimum then a perturbation will be linearly damped, although a finite-amplitude perturbation might grow. If χ_0 is a maximum then (A 5) guarantees linear instability of χ_0.

Appendix B. The structure of the internal boundary layers

The steady-state solutions satisfy the differential equation

$$V_\chi = \mu^2 \chi(\chi-\eta)^2 + \chi - rf = \gamma^2 \partial_y^2 \chi. \tag{B 1}$$

Steady boundary layers can only be found at the critical points, whose locations, y_S, are found by requiring that the areas P and Q in figure 1 are equal. Now the inflexion point, χ_I, of the cubic polynomial on the left-hand side of (B 1) is at

$$\chi_I \equiv \tfrac{2}{3}\eta. \tag{B 2}$$

From symmetry, the location of the critical point is determined by requiring that χ_I coincides with the middle zero of V_χ (i.e. χ_B in figure 1). Thus the locations of the critical points are given implicitly by

$$3rf(y_S) = 2\eta(1+\tfrac{1}{9}\mu^2\eta^2(y_S)). \tag{B 3}$$

(For instance, substituting $f(y)$ and $\eta(y)$ from (5.1) into (B 3) we get (5.3).) Since $f(y)$ varies slowly on the scale of the boundary layer we can use (B 3) to eliminate $f(y)$ from (B 1) and then factor the resulting cubic. Thus, in the vicinity of the critical points, the boundary-layer approximation of (B 1) is

$$\mu^2(\chi-\tfrac{2}{3}\eta)\,[(\chi-\tfrac{2}{3}\eta)^2+\mu^{-2}-\tfrac{1}{3}\eta^2] = \gamma^2\,\partial_y^2\chi. \tag{B 4}$$

The solution of (B 4) is

$$\chi = \tfrac{2}{3}+\alpha\tanh\left[\frac{y-y_S}{\delta}\right], \tag{B 5}$$

where we have made the definitions

$$\alpha^2 \equiv \tfrac{1}{3}\eta^2-\mu^{-2}; \quad \delta \equiv \frac{\sqrt{2\gamma}}{\mu|\alpha|} \ll 1. \tag{B 6}$$

Indeed, the outer limit of the boundary-layer solution is

$$\chi_{\pm\infty} = \tfrac{2}{3}\eta \pm \alpha. \tag{B 7}$$

These values of χ coincide with the (stable) zeros χ_A and χ_B of V_χ at the critical points location, y_S.

REFERENCES

Alikakos, N., Bates, P. W. & Fusco, G. 1991 Slow motion for the Cahn–Hilliard equation in one space dimension. *J. Diffl Equat.* **90**, 81–135.

Broecker, W. S., Peteet, D. M. & Rind, D. 1985 Does the ocean–atmosphere system have more than one stable mode of operation? *Nature* **315**, 21–26.

Bryan, F. 1986 High-latitude salinity effects and interhemispheric thermohaline circulations. *Nature* **323**, 301–304.

Cahn, J. W. & Hilliard, J. H, 1958 Free energy of a nonuniform system. I. Interfacial free energy. *J. Chem. Phys.* **28**, 258–267.

Chapman, C. J. & Proctor, M. R. E. 1980 Nonlinear Rayleigh–Bénard convection between poorly conducting boundaries. *J. Fluid Mech.* **101**, 759–782.

Depassier, M. C. & Spiegel, E. A. 1982 Convection with heat flux prescribed on the boundaries of the system. I. The effect of temperature dependence on material properties. *Geophys. Astrophys. Fluid. Mech.* **21**, 167–188.

Kennett, J. P. & Stott, L. D. 1991 Abrupt deep-sea warming, palaeoceanographic changes and benthic extinctions at the end of the Palaeocene. *Nature* **353**, 225–229.

Manabe, S. L & Stouffer, R. J. 1988 Two stable equilibria of a coupled ocean–atmosphere model. *J. Climate* **1**, 841–866.

Roberts, A. J. 1985 An analysis of near-marginal, mildly penetrative convection with heat flux prescribed on the boundaries. *J. Fluid Mech.* **158**, 71–93.

Stommel, H. M. 1961 Thermohaline convection with two regimes of flow. *Tellus* **13** (2), 224–230.

Taylor, G. I. 1953 Dispersion of soluble matter in solvent flowing slowly through a tube. *Proc. R. Soc. Lond.* A**219**, 186–203.

Thual, O. & McWilliams, J. C. 1991 The catastrophic structure of thermohaline convection in a two-dimensional fluid and a comparison with low-order box models. *Geophys. Astrophys. Fluid Dyn.* (in press).

Welander, P. 1986 Thermohaline effects in the ocean circulation and related simple models. In *Large-Scale Transport Processes in Oceans and Atmosphere* (ed. J. Willebrand & D. L. T. Anderson) pp. 163–200, NATO ASI Series. Reidel.